Process optimisation in deep drawing

Omar Ghouati — Jean-Claude Gelin — Henrik Lenoir

Laboratoire de Mécanique Appliquée R.Chaléat
UMR CNRS 6604, Université de Franche-Comté,
24 rue de l'Epitaphe, F-25000 Besancon

RÉSUMÉ. *On propose dans cet article une technique numérique d'optimisation de procédé appliquée à l'emboutissage des tôles minces. Cette technique est basée sur le couplage d'une méthode d'optimisation et d'une méthode de calcul par éléments finis permettant de simuler l'emboutissage des tôles minces. L'algorithme d'optimisation est basé sur une méthode de type gradient comprenant un module d'analyse de sensibilité et permet d'optimiser les paramètres de procédé de façon à ce que la pièce obtenue possède la géométrie souhaitée. Des exemples numériques sont présentés pour illustrer l'efficacité de l'approche proposée.*

ABSTRACT. *A numerical technique for process optimisation applied to the deep drawing of sheet metals is proposed in this paper. This technique is based on the combination of an optimisation algorithm and a finite element method. The optimisation algorithm is based on a gradient method containing a sensitivity analysis and allows to optimise process parameters in order to obtain a final product with the desired shape. Numerical examples are presented to illustrate the efficiency of the proposed approach.*

MOTS-CLÉS : *Optimisation, analyse de sensibilité, emboutissage*

KEY WORDS: *Optimisation, sensitivity analysis, deep drawing*

Revue européenne des éléments finis. Volume 9 – n° 1-2-3/2000, pages 129 à 149

1. Introduction

The design and control of forming processes require an accurate tuning of parameters having an effect on the behaviour of the process. These parameters can be classified into three main categories: operating conditions (punch load, blank-holder force, lubrication...), geometry (of the blank or the tools) and material (elastic properties, hardening and anisotropy). Empirical methods based solely on the experimental knowledge are no longer sufficient. Moreover, the development of numerical techniques allows profiting from the predictive capabilities of the finite element method in order to determine optimal process parameters.

In this paper, a numerical procedure is proposed for the design of deep drawing processes. It is based on the coupling of an optimisation technique and the finite element method. The optimisation technique allows adjusting the parameters such that specified criteria are fulfilled. The finite element method, in addition to providing the response of the process with fixed parameters, allows the assessment of the effect of a variation of these parameters on this response. This is achieved using a sensitivity analysis based on a direct differentiation method consistent with the finite element method formulation. The use of such a method allows an accurate sensitivity evaluation with the minimum extra cost in computation time. The simulation of a deep drawing process makes use of shell elements in two or three dimensions with a mixed interpolation for transverse shear components [BOU 96], [GEL 95]. Sheet material properties are described using elastoplastic behaviour, with or without anisotropy. Elastoplasticity is described using an orthotropic Hill criterion taking into account hardening and associate flow rule. Blank-holder actions on the sheet are modelled by penalising contact reactions in the case of implicit approaches, or by dynamic projection and local equilibrium in the case of dynamic explicit approaches. Springback is modelled using an unloading procedure [JOA 95].

2. Characterisation of deep drawing processes

To achieve the optimisation of deep drawing processes, it is necessary to define performance functions representing the quality of the obtained product. These functions are relevant to shape accuracy, surface distortions (buckling, wrinkling, scratching mark...), thickness distortions (thinning, ductile fracture, failure, diffuse and localised necking...). In a process optimisation context these functions are considered to be either objective functions or constraint functions. In the following, some examples of such functions are provided.

2.1. *Shape accuracy*

The function to be defined here has to represent the distance of the obtained product to its CAD definition, which is the desired shape. A general form for this function can be written as follows:

$$F_{SH} = \left(\sum_{i=1}^{n} \alpha \left(\frac{X_i^{CAD} - X_i^{NUM}}{X_i^{CAD}} \right)_+^p \right)^{\frac{1}{p}} + \left(\sum_{i=1}^{n} \beta \left(\frac{X_i^{NUM} - X_i^{CAD}}{X_i^{CAD}} \right)_+^q \right)^{\frac{1}{q}} \quad [1]$$

where: X^{CAD} represents the geometrical position given by the CAD model, X^{NUM} represents the geometrical position provided by the numerical simulation, n represents the number of positions in the product taken into account to evaluate the distance and therefore define an interest zone, α and β are weighting coefficients, p and q define the norm used to measure the distance, $(.)_+$ is an operator defined by: $(A)_+ = A$ if $A > 0$ and $A = 0$ if not. This operator allow distinguishing a quality which is different upper or under the value of X^{CAD}.

2.2. *Quality of the product*

An easy way to represent the quality of the deep drawn product is to use thickness distribution at the end of the process. The optimal conditions correspond to the case where no excessive thinning or thickening occurs in the area of interest for the product; thickening to some extent can be afforded in the region that will be subsequently trimmed away. A general form for the function representing the quality of the product can be written as follows [BAR 98]:

$$F_{QP} = \left(\sum_{i=1}^{n} \alpha \left(\frac{h_0 - h_i}{h_0} \right)_+^p \right)^{\frac{1}{p}} + \left(\sum_{i=1}^{n} \beta \left(\frac{h_i - h_0}{h_0} \right)_+^q \right)^{\frac{1}{q}} \quad [2]$$

with the same definitions as in equation [1] and where h_0 represents the initial sheet thickness and h_i represents the nodal thickness at node i.

This function takes into account thinning by means of the first term and thickening with the second term.

2.3. *Initial blank volume*

An important issue in deep drawing is the reduction of the amount of sheet residue. It is therefore desirable to use the minimal amount of initial sheet metal to get the final product. A general form for the function representing the initial blank volume can be written as follows:

$$F_{IV} = \sum_{e} A_e . h_e \qquad [3]$$

where A and h represent respectively element area and thickness.

2.4. *Punch/blank-holder forces*

Another important issue is the reduction of energy costs associated to the punch and blank-holder forces, the aim being their reduction. A function can be defined by introducing energies of punch and blank-holder compared to reference energy in the following form:

$$F_{CF} = \frac{\left(F_{punch} V_{punch} + F_{blank-holder} V_{blank-holder}\right)^p}{E_0} \qquad [4]$$

where F_{tool} and V_{tool} are respectively the force and the velocity of the considered tool and E_0 is the reference energy.

All the functions described above can be evaluated using a numerical method that provides accurate and reliable information. In this paper a finite element method is used. This allows predicting the shape of the final product as well as thickness, strain and stress distribution but also punch and blank-holder forces, for fixed process parameters. Furthermore, associated to this finite element method, a sensitivity analysis is developed on the basis of a direct differentiation consistent with the finite element formulation. This sensitivity analysis provides reliable and accurate information at a minimal extra-computation cost. It allows the determination of the effect of each variation of a process parameter on the function chosen to characterise the process.

The solution of the mechanical problem and the associated sensitivity analysis are described in the next section.

3. Objective and constraint functions evaluation

3.1. *Mechanical problem formulation and solution*

Consider a solid S occupying a domain Ω_0 with boundary Γ_0 in the initial configuration and the domain Ω with boundary Γ in the current configuration. On boundaries Γ_u and Γ_σ ($\Gamma_\sigma \cap \Gamma_u = \varnothing$, $\Gamma_\sigma \cup \Gamma_u = \Gamma$), the displacement vector $\bar{\mathbf{u}}$ and the traction vector $\mathbf{f}_s$ are prescribed. The solid undergoes a deformation process specified by the displacement field $\mathbf{u}_t(\mathbf{p},t)$ where t is time or a time like parameter for the quasistatic process and $\mathbf{p}$ is the vector of process parameters. In a finite deformation process the initial configuration C_0 is deformed into C_t with $\mathbf{x}_t = \mathbf{x}_0 + \mathbf{u}_t$.

The following weak form associated with the equilibrium equations for the sheet metal S is used in the finite element method:

$$\mathbf{G}(\mathbf{u}_t(\mathbf{p}),\eta) = \int_{\Omega_t} \mathbf{T}(\mathbf{u}_t(\mathbf{p})) : \nabla^s_{x_t} \eta dV - \int_{\Gamma_\sigma} (\bar{f}_s.\eta) dS = 0 \qquad [5]$$

where $\mathbf{T}$ is the Cauchy stress tensor, η is an homogeneous displacement field ($\eta=0$ over Γ_u) and $\nabla^s_{x_t}\eta$ is the symmetrical gradient of η in the current configuration.

Equation [5] is non-linear with respect to $\mathbf{u}_t(\mathbf{p})$. The solution process is performed using a Newton iterative scheme and leads to the following equation:

$$\int_{\Omega_t} \mathbf{C}(\nabla^s_{x_t}\mathbf{u}_t) : \nabla_{x_t}\delta\mathbf{u}_t : \nabla^s_{x_t}\eta dV + G(\mathbf{u}_t,\eta) = 0 \qquad [6]$$

where $\delta\mathbf{u}$ represents the displacement increment, $\mathbf{C}(\nabla^s_{x_t}\mathbf{u}_t(\mathbf{p}))$ represents the tangent operator consistent with the stress evaluation algorithm and internal variables.

In the displacement based finite element method, the discretized form of the equation [6] is used to calculate an estimated incremental displacement $\delta\mathbf{u}_{n+1}$ between t_n and t_{n+1}, following the implicit iterative equation:

$$[\mathbf{K}_T]^{(i)}_{n+1}\delta\mathbf{u}^{(i)}_{n+1} = \mathbf{F}_{ext} - [\mathbf{F}_\sigma(\nabla^s_{n+1}\mathbf{u}_t(\mathbf{p}))]^{(i)}_{n+1} \qquad [7]$$

where $\mathbf{F}_{ext}$ represents the nodal vector of external loads, $[\mathbf{F}_\sigma(\nabla^s_{n+1}\mathbf{u}_t(\mathbf{p}))]$ the nodal vector of internal loads, and $[\mathbf{K}_T]$ represents the tangent stiffness matrix. These quantities are given by the following expressions:

$$\begin{cases} [\mathbf{F}_\sigma(\nabla^s_{n+1}\mathbf{u}_t(\mathbf{p}))]^{(i)}_{n+1} = \int_{\Omega^{(i)}_{n+1}} (\mathbf{B}^{(i)}_{n+1})^T \mathbf{T}_{n+1}(\mathbf{u}_t(\mathbf{p}))dV \\ [\mathbf{K}_T]^{(i)}_{n+1} = \int_{\Omega^{(i)}_{n+1}} (\mathbf{B}^{(i)}_{n+1})^T \mathbf{C}(\nabla^S_{n+1}\mathbf{u}_t(\mathbf{p}))(\mathbf{B}^{(i)}_{n+1})dV \end{cases} \quad [8]$$

where **B** is the strain-displacement interpolation matrix.

In the case of the transient explicit solution procedure, the acceleration is taken into account, the virtual work principle can be written in an Eulerian manner as:

$$\int_{\Omega_t} \mathbf{T}(\mathbf{u}_t) : \nabla^s_{x_t} \eta dV - \int_{\Gamma_\sigma} (\overline{f_s}.\eta)dS + \int_{\Omega_t} \rho\gamma\eta dV = 0 \quad [9]$$

After discretisation, integral form [9] is transformed as:

$$\mathbf{M}_{n+1}\tilde{\mathbf{a}}_{n+1} = \mathbf{F}_{ext} - [\mathbf{F}_\sigma(\nabla^s_{n+1}\mathbf{u}_t(\mathbf{p}))]_{n+1} \quad [10]$$

where $\boldsymbol{\gamma}_{n+1}$ is the nodal accelerator vector and $\mathbf{M}_{n+1}$ the mass matrix.

Nodal accelerations vector is obtained by solving equation [10] and velocities, respectively displacements are obtained by a central difference formula. In the particular case where **M** is a diagonal matrix, the solution process is easy and fast.

3.2. *Sensitivity analysis*

A sensitivity analysis for metal forming problems has been developed on the basis of direct differentiation of the solution process for the mechanical problem [GHO 96], [GHO 98].

Sensitivity of displacements is obtained, in the implicit case, by solving the following equation:

$$\frac{d(\Delta\mathbf{u}_{n+1})}{d\mathbf{p}} = -\mathbf{K}_T^{-1}\left[\frac{\partial\mathbf{F}_\sigma}{\partial\mathbf{p}} - \frac{\partial\mathbf{K}_T}{\partial\mathbf{p}}\Delta\mathbf{u}_{n+1}\right] \quad [11]$$

The inverse of the stiffness matrix can be obtained from the solution of the direct problem. It remains therefore to evaluate the sensitivity of the stiffness matrix and the sensitivity of the internal load vector.

In the explicit case, the first stage is to evaluate sensitivity of the acceleration vector using the following equation:

$$\mathbf{M}_n \frac{d\tilde{\mathbf{a}}_{n+1}}{d\mathbf{p}} = \frac{d\mathbf{F}_{ext}}{d\mathbf{p}} - \frac{d\mathbf{F}_\sigma}{d\mathbf{p}} - \frac{d\mathbf{M}_n}{d\mathbf{p}} \tilde{\mathbf{a}}_{n+1} \qquad [12]$$

This equation provides sensitivity of the acceleration vector relative to process parameters at time t_{n+1} knowing sensitivity of the mass matrix, sensitivity of the external load vector and the sensitivity of the internal load vector, at time t_n. On the other hand, since the sensitivity analysis is performed once the mechanical problem has been solved, the quantities $\mathbf{M}_n$ and γ_{n+1} are known.

Next stage of the sensitivity analysis is the evaluation of sensitivities of the mass matrix, the internal load vector and the external load vector.

Sensitivity of the stiffness matrix and the mass matrix are given by the following expressions:

$$[\mathbf{K}_T]^{(i)}_{n+1} = \int_{\Omega^{(i)}_{n+1}} \frac{d\mathbf{B}^{T(i)}_{n+1}}{d\mathbf{p}} .\mathbf{C}.\mathbf{B}^{(i)}_{n+1} dV + \int_{\Omega^{(i)}_{n+1}} \mathbf{B}^{(i)\,T}_{n+1} \frac{d\mathbf{C}}{d\mathbf{p}} \mathbf{B}^{(i)}_{n+1} dV$$
$$+ \int_{\Omega^{(i)}_{n+1}} \mathbf{B}^{(i)\,T}_{n+1} \mathbf{C} \frac{d\mathbf{B}^{(i)}_{n+1}}{d\mathbf{p}} dV + \int_{\Gamma^{(i)}_{n+1}} \mathbf{B}^{(i)\,T}_{n+1} .\mathbf{C}.\mathbf{B}^{(i)}_{n+1} \frac{d\mathbf{u}_n}{d\mathbf{p}} \vec{\mathbf{n}} dS \qquad [13]$$

$$\frac{d\mathbf{M}_n}{d\mathbf{p}} = \int_{\Omega(p)} \frac{d\rho}{d\mathbf{p}} \mathbf{N}^T \mathbf{N} dV + \int_{\Omega(p)} \rho \frac{d\mathbf{N}^T}{d\mathbf{p}} \mathbf{N} dV + \int_{\Omega(p)} \rho \mathbf{N}^T \frac{d\mathbf{N}}{d\mathbf{p}} dV + \int_{\Gamma(p)} \rho \mathbf{N}^T \mathbf{N} \frac{d\mathbf{u}_n}{d\mathbf{p}} \vec{\mathbf{n}} dS \qquad [14]$$

where $\vec{\mathbf{n}}$ is the external unit vector to the boundary Γ of the domain under consideration.

Sensitivity of the internal load vector expresses as follows:

$$\frac{d\mathbf{F}_\sigma}{d\mathbf{p}} = \int_{\Omega(p)} \frac{d\mathbf{B}^T}{d\mathbf{p}} \mathbf{T}_n dV + \int_{\Omega(p)} \mathbf{B}^T \frac{d\mathbf{T}_n}{d\mathbf{p}} dV + \int_{\Gamma(p)} \mathbf{B}^T \mathbf{T}_n \frac{d\mathbf{u}_n}{d\mathbf{p}} \vec{\mathbf{n}} dS \qquad [15]$$

Expression of the sensitivity of the external load vector is:

$$\frac{d\mathbf{F}_{ext}}{d\mathbf{p}} = \int_{\Gamma_\sigma(p)} \frac{d\mathbf{N}^T}{d\mathbf{p}} \overline{\mathbf{f}_s} dS + \int_{\Gamma_\sigma(p)} \mathbf{N}^T \frac{d\overline{\mathbf{f}_s}}{d\mathbf{p}} dS + \int_{\partial\Gamma_\sigma(p)} \mathbf{N}^T \overline{\mathbf{f}_s} \frac{d\mathbf{u}_n}{d\mathbf{p}} \vec{\mathbf{n}} dl \qquad [16]$$

In these expressions, sensitivity of the Cauchy stress tensor is needed and evaluated in a consistent manner with the algorithm of evaluation of stresses and internal variables.

4. Optimisation problem formulation

Process optimisation is formulated as a non-linear mathematical programming problem in the following form [GHO 96; KEG 95; SCH 94]:

$$\min_{p} S_0(\mathbf{p},\mathbf{u}) \qquad [17]$$

subject to constraints:

$$\begin{cases} h_j(\mathbf{p},\mathbf{u}) \le 0 & 1 \le j \le n_{ic} \\ g_i(\mathbf{p},\mathbf{u}) = 0 & 1 \le i \le n_c \end{cases} \qquad [18]$$

where n_{ic} are the number of inequality constraints and n_c the number of equality constraints, $\mathbf{p}$ represents the vector of process parameters and $\mathbf{u}$ the calculated displacement field.

The objective function S_0 is a process performance measure, whereas the constraint functions are introduced in order to take into account technology limitations such as bounds on the process parameters.

4.1. *Local search optimization method*

In this approach, a FSQP method [LAU 97] is used in order to solve the problem associated to equation [1]. This method allows satisfying the constraints during the optimisation ensuring that no unrealistic values for the parameters are used in the finite element method.

4.2. *Response surface approach*

This is a two-stage approach. First, approximations for the objective and constraint functions are constructed, then an optimisation algorithm is used to solve the problem of equation [17] using these approximations. Functions $S_0(p)$, $h(p)$ and $g(p)$ are therefore replaced in equation [17] by global approximations $S_a(p)$, $h_a(p)$ and $g_a(p)$ determined using a finite number of simulations performed for different values of p. This response surface approach obtained by numerical simulation is

reported in [ROU 98], [SCH 98]. This method allows simplifying the sensitivity analysis necessary for the optimisation algorithm used (SQP). Furthermore, it allows to explore, from the beginning, a very large domain for p. Polynomial expressions of degree n are used for $S_a(p)$, $h_a(p)$ and $g_a(p)$ in the following form:

$$f_a(x) = c_f^T\, y \qquad [19]$$

where f is a generic notation representing S, h or g, y vector of monomials evaluated in $\mathbf{p}$ and c_f coefficient vector, both of dimension k_f.

The number of simulations to perform in order to identify c_f is chosen around 1.5 to 3 times $\max(k_f)$. The corresponding values of $\mathbf{p}$ are extracted from experimental designs built following a D-optimal criterion using the Gosset software [HAR 94]. The coefficients are evaluated in a least-squares sense by minimising the following sum:

$$\sum_{i=1}^{P}\left[f(x_i) - f_a(x_i)\right]^2 = \sum_{i=1}^{P}\left[f(x_i) - c_f^T y\right]^2 \qquad [20]$$

where P is the number of test points.

The coefficients vector c_f is obtained by:

$$c_f = (Y^T Y)^{-1} Y^T f \qquad [21]$$

where f is a column vectors of $f(\mathbf{p}_i)$ and Y is a matrix formed by the $y(\mathbf{p}_i)$.

More simulations are performed in order to check the validity of the model. In case of large prediction errors, c_f must be recalculated using a set of test points deduced from the previous one.

The convergence of the algorithm is not guaranteed in every case. The main cause is the choice of a large domain of study. In this case functions S_0, h and g might present very strong non-linearities. An automatic procedure for domain reduction can be considered in this case [ROU 98].

5. Applications

5.1. *Optimisation of a circular sheet*

The first example concerns the optimisation of the radius of a circular sheet with initial thickness of 0.7 mm, in order to reduce thickness variations at the end of the process [BAR 98]. The geometry of the test is reported in figure 1.

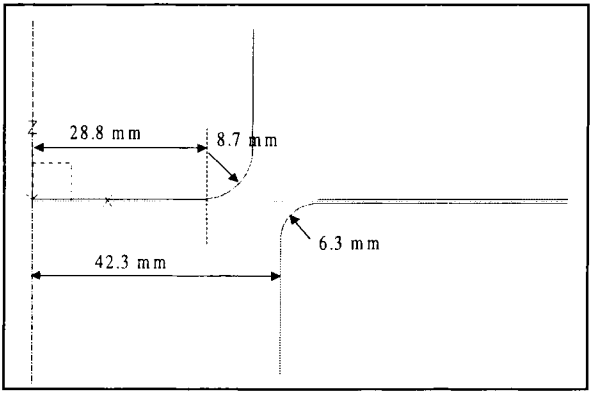

Figure 1. *Geometry of the drawing of a circular sheet*

A Swift hardening function represents material law for the sheet metal:
$\bar{\sigma} = 729.09\left(0.0135 + \bar{\varepsilon}_p\right)^{0.1657}$ MPa.

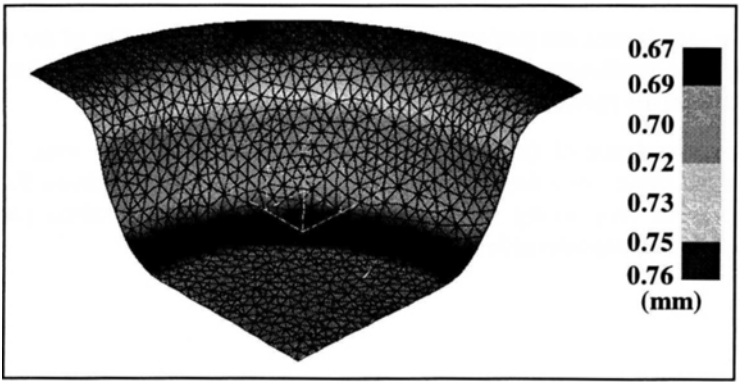

Figure 2. *Thickness distribution for a sheet radius of 65.0 mm*

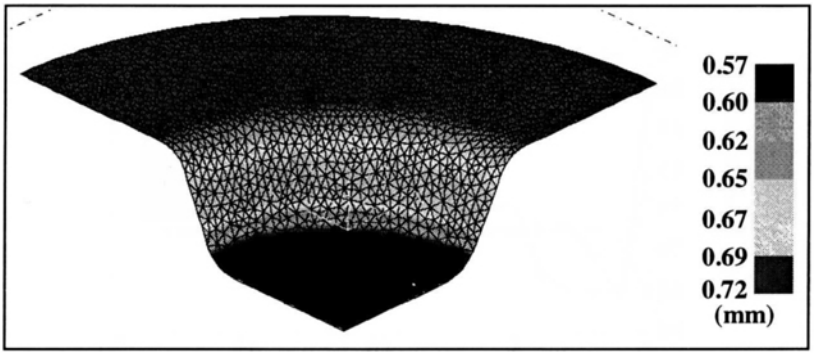

Figure 3. *Thickness distribution for a sheet radius of 90.0 mm*

Due to the symmetry of the problem and assuming isotropic behaviour, only one quarter of the part was discretised using triangular shell elements. Figures 2 and 3 represent thickness distribution for a sheet radius of respectively 65 mm and 90 mm.

It can be noticed that for a small initial sheet radius (65 mm), the thickening is excessive even if the thinning remains moderate. On the other hand, for an initial radius of 95 mm, if the thickening is reduced, the thinning is simultaneously increased. The goal of the optimisation is therefore here to find the optimal initial blank radius leading to the best compromise between thinning and thickening.

Among different possible forms, the following objective function provides the best results:

$$S_0 = \sum_{i=1}^{NbN} \left| \frac{h_i - h_0}{h_0} \right|^2 \qquad [22]$$

where NbN is the total number of nodes, h_i is the nodal thickness at the end of the process and h_0 is the initial thickness.

Both methods of optimisation described in Section 4 were used to solve this problem.

5.1.1. *Local search method*

A FSQP method was applied to solve the optimisation problem with the objective function described in equation [22]. Different values for the initial parameter guess were tried to ensure that the solution obtained is the global minimum.

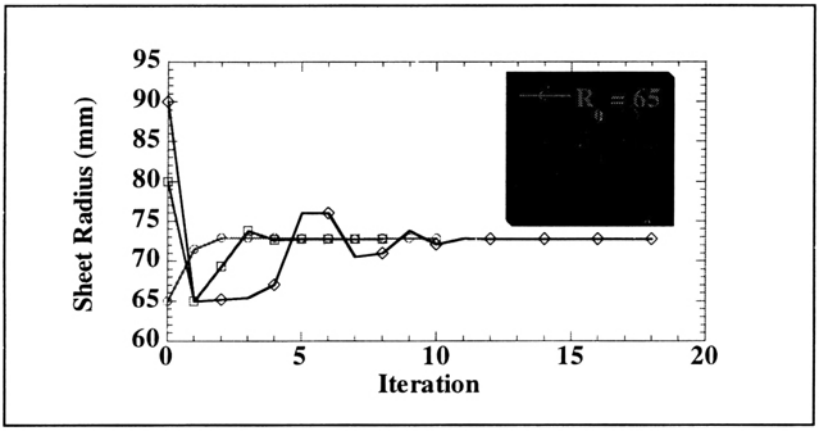

Figure 4. *Evolution of the process parameter during optimisation*

Figures 4 and 5 represent respectively the evolution of the objective function and the parameter (blank radius) during the optimisation procedure. As can be noticed, as the initial guess gets farther from the solution, it takes more time for the iterative process to converge.

In order to cross-correlate these results, thickness distributions for the optimal value are compared with those for the upper and lower bound on the parameter in figure 6. It can be seen that thickness distribution is indeed more homogeneous.

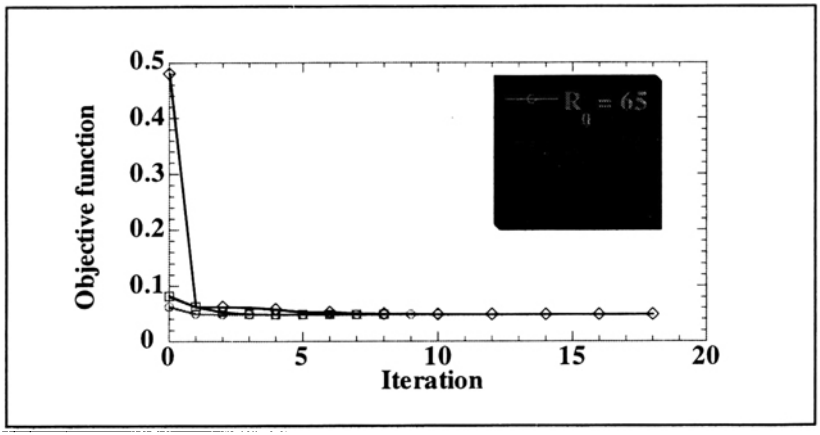

Figure 5. *Evolution of the objective function during optimisation*

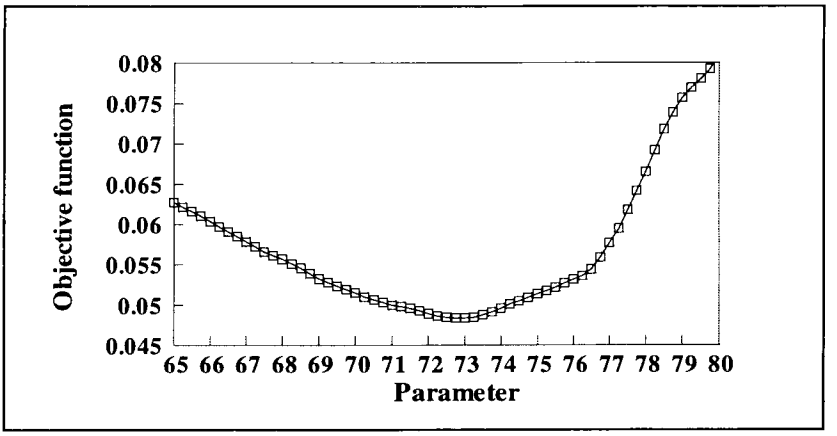

Figure 6. *Thickness distribution for bounds and optimal value of the process parameter*

The example studied here is a very simple one that allows easily to verify the results obtained. To do so, the objective function can be plotted with respect to the process parameter (figure 7).

It can be noticed that the optimal value for this problem is in deed R_{opt} = 72.8 mm.

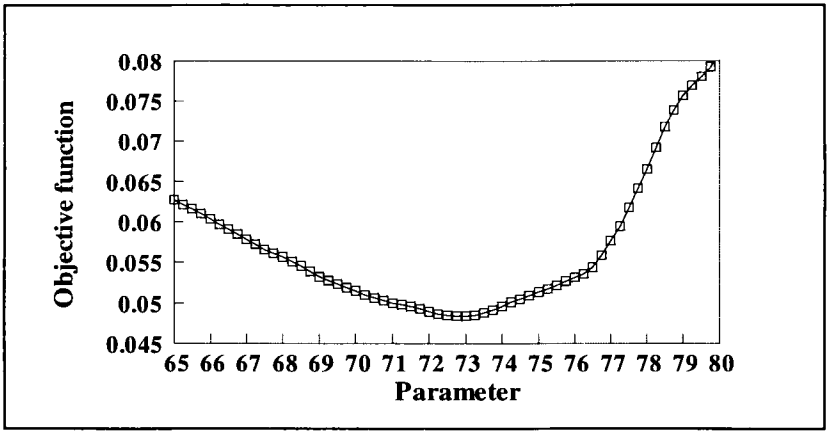

Figure 7. *Evolution of the objective function with respect to the process parameter*

5.1.2. *Response surface approach*

A quadratic approximation is used for the objective function following the expression:

$$S_0 = a_0 + a_1.p + a_2.p^2 \qquad [23]$$

where a_i are polynomial coefficients to identify and p represents the process parameter.

To be able to identify coefficients a_i (i=1, 2, 3), a minimal number of three simulations is sufficient. However, in order to study the effect of the number of simulations on the optimisation results, four cases where studied: 3, 5, 9 and 17 simulations respectively. The results obtained from the approximations constructed with each case are reported in Table 1. It can be noticed that from nine simulations the approximation constructed leads to an optimal parameter close enough to the actual value (less than 1-% error). This is to be added to the fact that in doing so, the number of simulations is limited and the optimisation process is highly simplified. Furthermore, with this method the problem of the initial guess is no longer present as the whole domain of solutions is explored from the beginning.

Of course, the example studied here is very simple but it does allow us to draw some conclusions as to the efficiency of the response surface approach compared to a classical local search method.

Number of simulations	Optimal parameter	Error in % (from the value 72.8 mm)
3	71.3	2.0
5	72.1	1.0
9	72.4	0.5
17	72.5	0.4

Table 1. *Results of the optimisation using different numbers of simulations to approximate the objective function*

5.2. *Optimisation of tool geometry*

One crucial problem in deep drawing is to determine the optimal tool geometry in order to achieve a desired shape for the component. This problem is addressed in

the second example. This is a U-bending test with a geometry represented in Figure 8 that was provided as a benchmark problem in NUMISHEET'93 Conference [MAK 93].

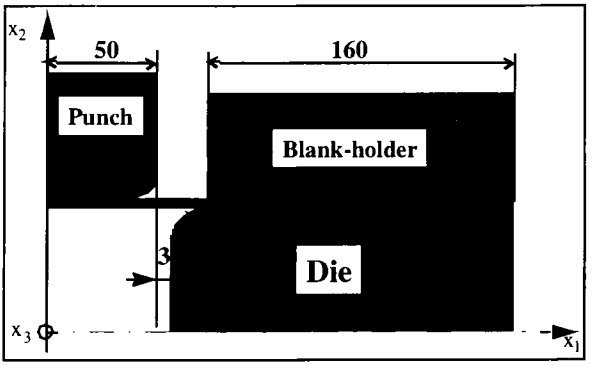

Figure 8. *Geometry of the U-bending test*

The material considered is a mild steel with behaviour represented by the following hardening law:

$$\sigma = K(\bar{\varepsilon}^{p})^{n} \qquad [24]$$

Geometry and material properties for this test are reported in table 2.

Property	**Value**
Initial sheet length (mm)	420.0
Initial sheet width (mm)	200.0
Initial sheet thickness (mm)	0.87
Young Modulus E (MPa)	206 800.0
Poisson's ratio ν	0.29
Yield stress σ_Y (Mpa)	160.0
K (MPa)	563.0
n	0.256
Blank-holder Force (kN)	100.0

Table 2. *Geometry and material properties for the U-bending test*

The direct problem was solved using shell elements. Among different possible forms, the following objective function proved to be the most efficient:

$$S_0 = \underset{i}{\text{Max}}\, d_i \qquad [25]$$

where d_i represents the distance from node i to the desired shape.

The goal of the optimisation here is to find the desired shape given by Figure 9.

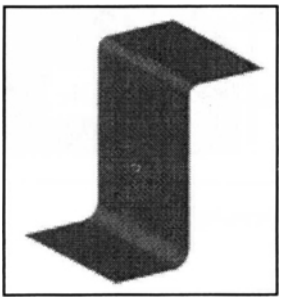

Figure 9. *Desired shape for the product after drawing*

Figure 10 represents the initial geometry of tools considered.

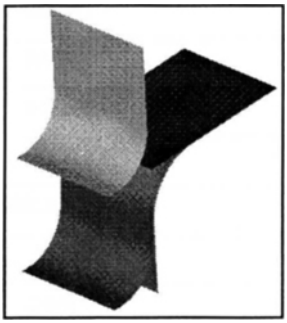

Figure 10. *Initial geometry of tools*

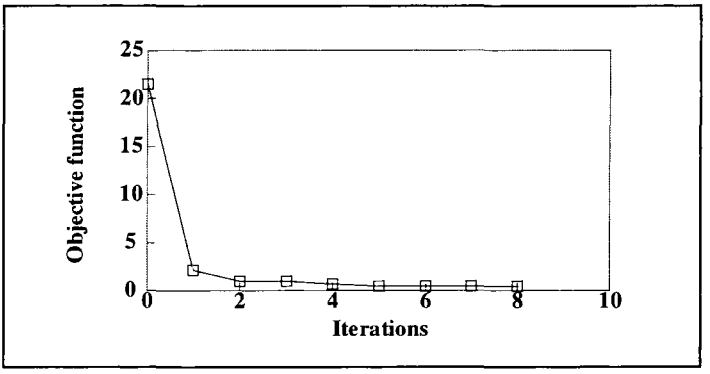

Figure 11. *Evolution of the objective function during optimisation*

Figure 11 represents the evolution of the objective function whereas figure 12 represents evolution of the parameters (punch radius and die radius) during the optimisation. A solution is achieved in six iterations.

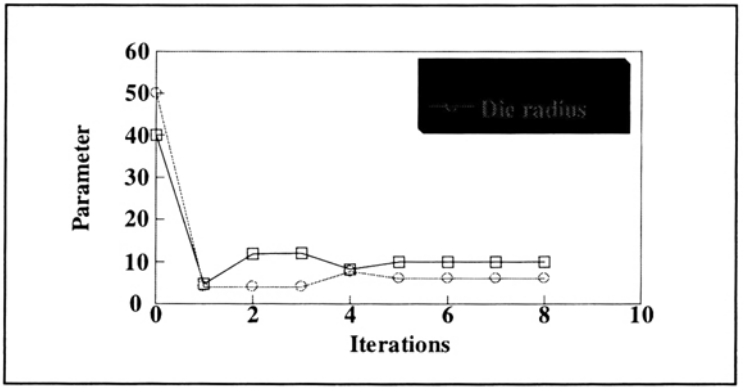

Figure 12. *Evolution of the process parameters during optimisation*

5.3. *Optimisation of initial blank volume*

In this example the goal is to find the minimal blank allowing the formability of a component. The component is a square box with a geometry represented in Figure 13 and was provided as a benchmark problem in NUMISHEET'93 Conference [MAK 93]. The initial thickness of the blank is 0.78 mm and a Swift hardening function represents material law for the sheet metal:

$$\bar{\sigma} = 729.09\left(0.0135 + \bar{\varepsilon}_p\right)^{0.1657} \text{MPa}.$$

Due to the symmetry of the problem and assuming isotropic behaviour, only one quarter of the part was discretised using triangular shell elements.

The optimisation for this example can be formulated as follows:

$$\text{minimise} \quad S_0 = \sum_e A_e h_e$$

$$\text{subject to} \quad \begin{cases} \dfrac{\text{Max}\, h_i - h_0}{h_0} \leq \text{htol}_{up} \\ \dfrac{\text{Min}\, h_i - h_0}{h_0} \geq -\text{htol}_{low} \end{cases} \qquad [26]$$

where A_e and h_e are respectively initial area and initial thickness for each finite element of the discretisation of the blank, h_0 is the initial thickness, h_i is the nodal thickness and htol_{up} and htol_{low} are tolerances respectively for thickening and thinning.

The objective function S_0 represents the volume of the initial blank whereas thickness is considered only in the useful zone of the final component (figure 13).

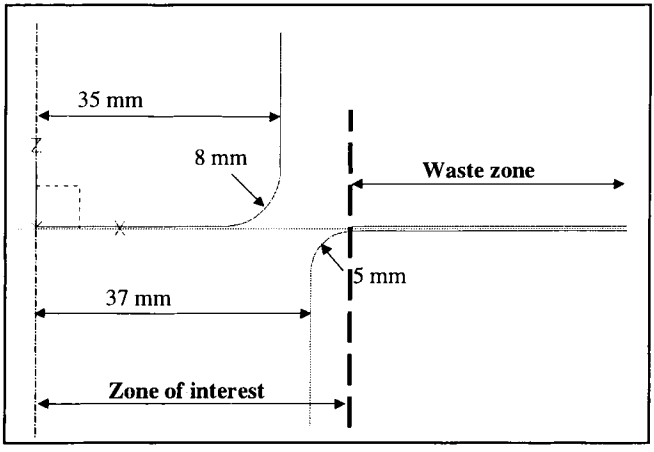

Figure 13. *Geometry of the square box test*

The initial blank is described by a B-spline curve defined using seven control points (figure 14). Positions of these control points represent process parameters for this example.

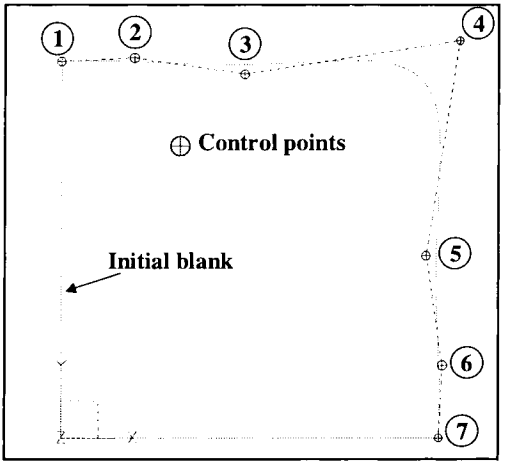

Figure 14. *Starting estimation for the initial blank shape and positions of the control points*

The following considerations have to be taken into account for the determination of the number of independent parameters that starts with a value of 14. Due to symmetries with respect to OX and OY axes, points 7 and 1 can only vary respectively along OX and OY reducing therefore the number of parameters to 12. On the other hand, as the final component is symmetrical and assuming isotropic behaviour, displacement of control points on each side are dependent. This means that for instance Y-displacement of point 2 is the same as X-displacement of point 6, and so on until point 4 where X-displacement and Y-displacement are the same. This second consideration reduces the number of independent parameters to 6. The final consideration is the fact that points 2 and 3 are constrained to move only in the Y-direction (respectively points 5 and 6 move only in the X-direction). The number of independent parameters is therefore 4 and the vector of process parameters is $\mathbf{p} = \{y_1, y_2, y_3, y_4\}^T$.

After each modification, the geometry is meshed keeping the same element size in order to minimise effects of the meshing on the results.

Only the local search technique was used for this example and provided the optimal geometry represented in Figure 15.

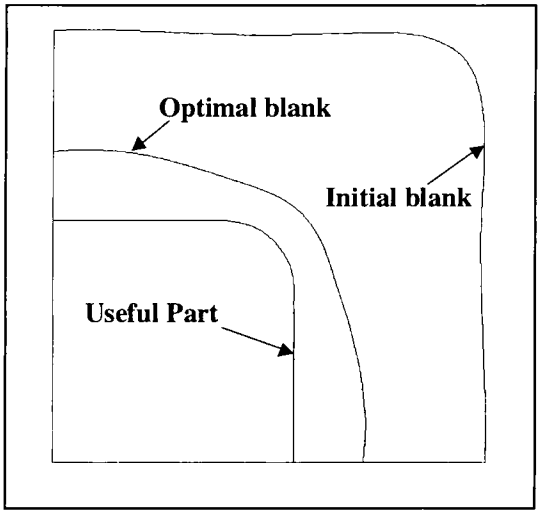

Figure 15. *Optimal shape for the initial blank*

After deformation, the waste zone is reduced as can be seen in Figure 16 where a deformed mesh is represented along with the contour of the useful zone.

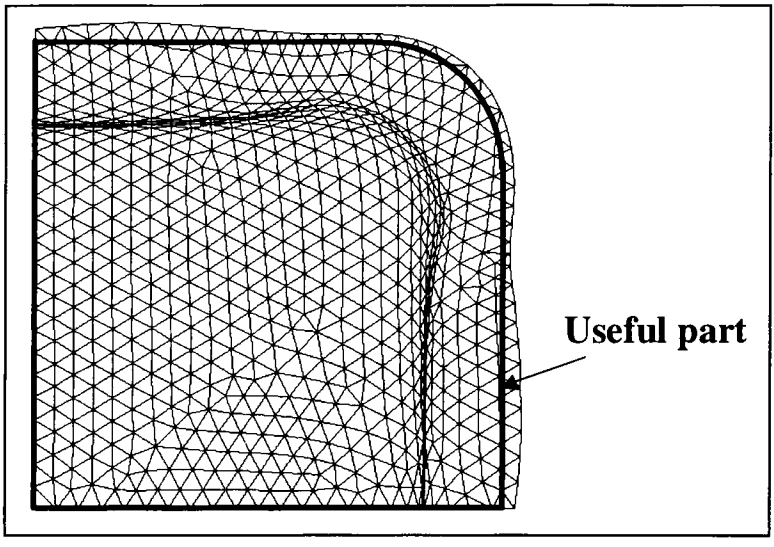

Figure 16. *Deformed mesh for the optimal blank.*

6. Conclusions

In this paper, a procedure for the design of forming processes is presented. The optimisation is performed by means of a gradient-based method including sensitivity analysis. First results obtained are promising in terms of convergence rates. Current works include the investigation of the use of sensitivity analysis in the construction of approximations used in surface response.

7. References

[BAR 98] BARLET O., Contribution à l'optimisation de forme de pièces embouties pour l'industrie automobile, Doctor Thesis (in French), UTC, 1998.

[BOU 96] BOUBAKAR L, BOULMANE L, GELIN J.C., "Finite element modelling of the stamping of anisotropic sheet metals", *Engineering Computations,* vol. 13, p. 143-171, 1996.

[JOA 95] JOANNIC D, GELIN J.C., Accurate simulation of springback in 3D sheet metal forming processes, *5th Int. Conf. on Numerical Methods in Industrial Forming Processes - Numiform'95,* Ed. by S.F. Shen and P.R. Dawson, A.A. Balkema Publ., 729-735, 1995.

[GEL 95] GELIN J.C., BOULMANE L., and BOISSE P., Quasi-static implicit transient analyses of sheet metal forming using a C0 three node shell element, J. Mater. *Processing Technology,* vol. 50, n° 1-4, 54-69, 1995.

[GHO 96] GHOUATI O., GELIN J.C., "Sensitivity analysis and optimization of shape and process parameters in metal forming", *Engineering Systems Design and Analysis Conference 1996,* vol. 3, p. 221-226.

[GHO 98] GHOUATI O., GELIN J.C., "Sensitivity analysis in forming processes", *International Journal of Forming Processes,* Vol.1, n°3/1998, p.297-322, (1998).

[HAR 94] HARDIN, R.H.; SLOANE, N.J.A.: *Operating manual for Gosset: a general purpose program for constructing experimental designs* (second edition), Mathematical Sciences Research Center, AT&T Bell Laboratories, 1994.

[KEG 95] KEGL M., BUTINAR B.J., OBLAK M.M., "Shape optimal design of elastic planar frames with non-linear response", *Int. J. Numer. Methods. Eng.,* vol. 38, 3227-3242, (1995).

[LAU 97] LAURENCE C., ZHOU J.L., TITS A.L, "User's guide for CFSQP Version 2.5", 1997.

[MAK 93] MAKINOUCHI A., NAKAMACHI E., Numisheet'93, *Numerical methods for sheet metal forming,* Tokyo, Japan, 1993.

[ROU 98] ROUX W.J.; STANDER N.; HAFTKA R.T.: "Response surface approximations for structural optimization", *Int. J. Num. Meth. Eng.,* 42, p. 517-534, 1998.

[SCH 94] SCHRAMM O., PILKEY W. D., "Optimal shape design for thin-walled beam cross-sections", *Int. J. Numer. Methods. Eng.,* vol. 37, 4039-4058, (1994).

[SCH 98] SCHIMMERLING P.; SISSON J.C.; ZAÏDI A.: Pratique des plans d'expériences, TEC & DOC, Paris, 1998.